ACS APPLIED MATERIALS & INTERFACES

Research Article

www.acsami.org

Organic Nanowire/Crystalline Silicon *p*–*n* Heterojunctions for High-Sensitivity, Broadband Photodetectors

Wei Deng, Jiansheng Jie,* Qixun Shang, Jincheng Wang, Xiujuan Zhang,* Shenwen Yao, Qing Zhang, and Xiaohong Zhang*

Institute of Functional Nano & Soft Materials (FUNSOM) and Collaborative Innovation Center of Suzhou Nano Science and Technology, Jiangsu Key Laboratory for Carbon-Based Functional Materials & Devices, Soochow University, Jiangsu, Suzhou 215123, China

Supporting Information

ABSTRACT: Organic/inorganic hybrid devices are promising candidates for high-performance, low-cost optoelectronic devices, by virtue of their unique properties. Polycrystalline/amorphous organic films are widely used in hybrid devices, because defects in the films hamper the improvement of device performance. Here, we report the construction of 2,4-bis[4-(*N*,*N*-dimethylamino)phenyl]squaraine (SQ) nanowire (NW)/crystalline Si (*c*-Si) *p*–*n* heterojunctions. Thanks to the high crystal quality of the SQ NWs, the heterojunctions exhibit excellent diode characteristics in darkness. It is significant that the heterojunctions have been found to be capable of detecting broadband light with wavelengths spanning from ultraviolet (UV) light, to visible (Vis) light, to near-infrared (NIR) light, because of the complementary spectrum absorption of SQ NWs with Si. The junction is demonstrated to play a core role in enhancing the device performance, in terms of ultrahigh sensitivity, excellent stability, and fast response. The photovoltaic characteristics of the heterojunctions are further investigated, revealing a power conversion efficiency (PCE) of up to 1.17%. This result also proves the potential of the device as self-powered photodetectors operating at zero external bias voltage. This work presents an important advance in constructing single-crystal organic nanostructure/inorganic heterojunctions and will enable future exploration of their applications in broadband photodetectors and solar cells.

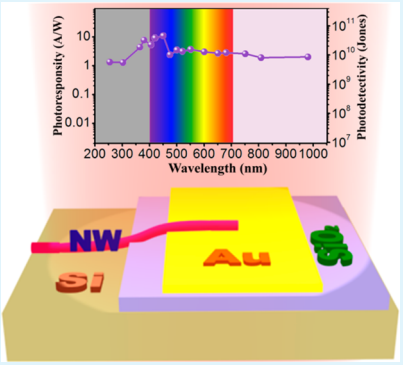

KEYWORDS: *organic nanowires, crystalline silicon, p–n heterojunctions, broadband photodetectors, solar cells*

INTRODUCTION

Photodetectors are a type of optoelectronic device for sensing light; they have found broad applications in consumer electronics, industrial security, space exploration, and the military.[1] It would be of great interest to make those photodetectors broadband for innovative applications. For example, broadband photodetectors could be loaded in a spectrometric analyzer so that one photodetector can detect light over a spectrum, from ultraviolet (UV), to visible (Vis), to infrared (IR). Crystalline silicon (*c*-Si) remains the dominant material for photodetector applications, such as charge-coupled devices (CCDs),[2,3] because of its high electronic mobility, which endows the devices with high sensitivity. However, its inherent properties, such as no absorption in the UV–IR band and low absorption coefficient in the Vis regime, make it incapable for use in broadband photodetectors. Notably, one-dimensional (1D) single-crystal organic nanostructures have attracted increasing interest, because of their tunable optical and electronic properties via molecular design. Their successful applications in photodetectors,[4−8] field-effect transistors (FETs),[9,10] and photovoltaics[11] makes them ideal building blocks for the next generation of high-performance electronic and optoelectronic devices. Among them, photodetectors based on small-molecule organic nanostructures have drawn particular attention, because of their much broader response spectra, compared to their inorganic counterparts, as well as their significantly higher sensitivity than that of their bulk and film materials.[6] They would find important applications in imaging,[12] optical communication,[13,14] and memory storage.[15−17] However, the improvement of the device performance is still hindered by the intrinsic low charge carrier density and low efficient carrier separation in organic materials.[4−7,18]

Organic/inorganic hybrid devices provide an ideal opportunity to combine the unique properties of both organic and inorganic materials. To date, many groups have reported the construction of organic/inorganic hybrid heterojunctions,[19−22] and demonstrated the improved device performances benefited from the utilization of the hybrid heterojunctions. Inorganic materials can produce large charge densities in device channels, because of their high electronic mobilities, while the existence of organic/inorganic heterojunction can effectively broaden the response spectrum range and facilitate the charge transport/separation as well, thus leading to enhanced performance.[23−26] However, most previously reported organic/inorganic hetero-

Received: November 12, 2014
Accepted: December 29, 2014
Published: December 29, 2014

DOI: 10.1021/am5079144
ACS Appl. Mater. Interfaces 2015, 7, 2039–2045

junctions usually involve the use of organic thin films, because of their easy accessibility by solution or evaporation process, which are not ideal charge-transport media, given their low mobility and greater number of structural defects, and, thus, inferior electronic performance.[9] Considering the combined merits of *c*-Si and single-crystal organic nanostructures, it is expected that their hybrid photodetectors would exhibit desirable device performance.

Herein, for the first time, we demonstrate the construction of single-crystal organic nanostructure/inorganic heterojunctions consisting of 2,4-bis[4-(*N*,*N*-dimethylamino)phenyl]squaraine (SQ) NWs and crystalline Si (*c*-Si). Significantly, the heterojunctions exhibited great promise as high-sensitivity broadband photodetectors, with spectrum response ranging from UV light, to Vis light, to near-infrared (NIR) light. The pronounced photovoltaic behavior of the heterojunctions was also observed, which made them excellent candidates for self-powered photodetectors. This work demonstrated the great potential of the single-crystal organic nanostructure/inorganic *p*−*n* heterojunctions in high-performance optoelectronic devices.

EXPERIMENTAL DETAILS

The stepwise process for the construction of the SQ NW/*c*-Si *p*−*n* heterojunction is shown in Figure S3 in the Supporting Information. A SiO_2 (300 nm)/*n*-Si (resistivity of <0.02 Ω cm) substrate was used. Photolithography, followed by wet etching with a buffered oxide etch (BOE) solution at room temperature, was performed to define SiO_2 insulating pads (250 μm × 250 μm) on the Si substrate. Then, 50 nm Au electrodes with a smaller size (200 μm × 200 μm), which served as the ohmic contacts to the SQ NWs, were fabricated on the SiO_2 pads by additional photolithography and lift-off processes. In a typical drop-casting experiment, SQ was first dissolved in dichloromethane (CH_2Cl_2) with a concentration of 0.05 mM. After that, 100 μL of SQ solution was drop-cast onto the *n*-type Si substrate under ambient air at room temperature (298 K). The solution would totally be evaporated within 1 min. The self-assembly of SQ molecules along the "π−π stacking" direction during the solution evaporation led to the formation of SQ NWs. The self-assembly of SQ molecules along the "π−π stacking" direction led to the formation of SQ NWs. By carefully controlling the growth conditions, such as the solution concentration and the amount of the solution applied on the device substrate, a portion of NWs would cross over both the exposed Si substrate and the Au electrodes, forming the heterojunctions through contact with the Si substrate. Also, the density of the SQ NWs was carefully controlled to ensure that a majority of the devices had only 1−2 SQ NWs on them. During measurements, we first inspected the devices using an optical microscope and then selected the devices with just one NW for further measurements.

Morphologies of the SQ NWs were investigated using scanning electron microscopy (SEM) (FEI, Model Quanta 200 FEG). The UV-vis absorption spectra were measured with an UV-vis spectrophotometer (Perkin−Elmer, Model Lambda 750). Electrical measurements on the devices were conducted with a semiconductor characterization system (Keithley, Model 4200). Monochromatic light in the UV-visible range was obtained by filtering the white light from a high-power xenon lamp with optical filters, and a power meter was used to determine the light intensity. Laser diodes with wavelengths of 808 and 980 nm were also used as the NIR light sources. To measure the photovoltaic characteristics, a solar simulator (Newport, Model 91160) equipped with a 300 W xenon lamp and an air mass (AM) 1.5 filter was used to generate simulated AM 1.5G solar irradiation (100 mW/cm^2).

RESULTS AND DISCUSSION

SQ is a typical organic dye with a very high extinction coefficient, which finds wide applications in diverse fields, such as photodetectors, sensors, solar cells, and so on.[9,27] It is known that both ground and excited states of SQ are intramolecular donor−acceptor−donor charge-transfer (D−A−D CT) states.[4] This type of molecule can easily aggregate and grow into 1D nanostructures in a "π−π stacking" arrangement directed by the strong intermolecular interactions between the acceptor (A) and the donor (D) groups under appropriate conditions.[28,29] Figure 1a shows the SEM image of SQ NWs obtained by a simple drop-casting method. Typically, the SQ NWs have a uniform width of 500−600 nm, a thickness of ∼40 nm, and a length of ∼150 μm. To assess the electrical characteristics of the SQ NWs, back-gate FETs based on individual SQ NW were constructed, revealing a hole mobility of 0.12 cm^2/(V s) for the NW (see Figure S1 in the Supporting Information). Furthermore, SQ NW/*c*-Si *p*−*n* heterojunctions were fabricated by simply dropping the SQ solution onto the *n*-type Si substrate with a predefined electrode and insulator layer (details for the fabrication procedure can be found in Figure S2

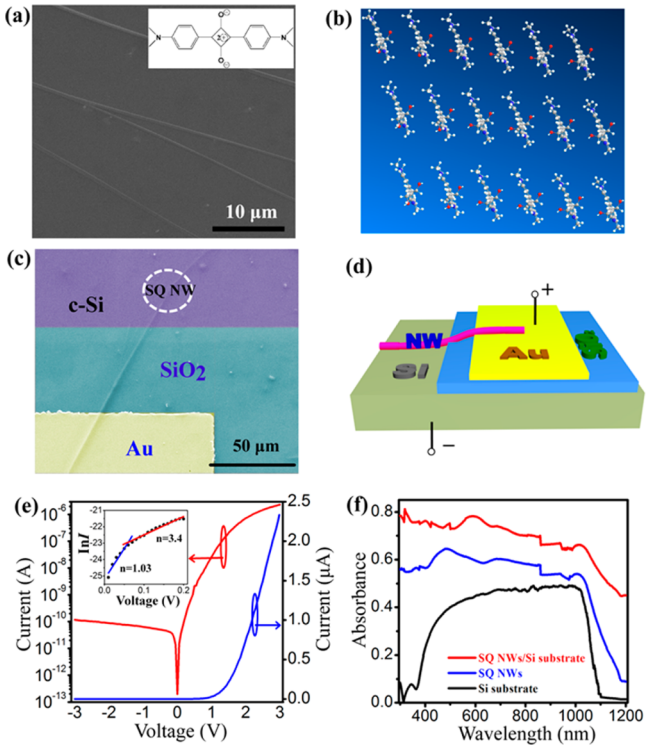

Figure 1. (a) SEM image of the SQ NW grown by drop-casting the SQ solution on a smooth silicon substrate; the inset shows the molecule structure of SQ. (b) Schematic representation of the crystal structure of the SQ NW. (c) SEM image and (d) schematic illustration of the SQ NW/*c*-Si heterojunction device. (e) Rectification characteristics of the SQ NW/*c*-Si *p*−*n* heterojunction measured in darkness; the inset shows the semilogarithmic plot of current versus bias voltage of the heterojunction, and the ideality factors (*n*) are deduced by fitting the curve with straight lines in the low-voltage and high-voltage regions, respectively. (f) Absorption spectra of the Si substrate, SQ NWs on Si substrate, and SQ NWs on quartz substrate, respectively; the SQ NWs show complementary spectrum absorption with Si, leading to the broadband absorption of the SQ NWs/Si combined system from ultraviolet (UV) light, to visible (Vis) light, to near-infrared (NIR) light.

DOI: 10.1021/am5079144
ACS Appl. Mater. Interfaces 2015, 7, 2039−2045

in the Supporting Information). This method allows the one-step NWs growth and device fabrication. Figure 1c displays the SEM image of a typical device with a single SQ NW crossing over the *n*-type Si substrate. One side of SQ NW contacts with *c*-Si directly, the other side lies on the SiO_2 layer with predefined Au electrode, as shown in the scheme of the heterojunction (Figure 1d). We note that a thin natural oxide layer (2−5 nm) may exist between the *n*-type Si substrate and the SQ NW, because of oxidation of the Si substrate in air. However, it is expected that the thin oxide layer will not have significant influence on the device performance, since it can allow the transportation of carriers via a tunneling effect. In addition, the growth of SQ NWs in our experiment was conducted at once after the BOE etching of the SiO_2/Si substrate, so that the natural oxide layer should not be too thick. The following electrical measurements also prove that the influence of the natural oxide layer on the device characteristics is negligible. Figure 1e shows the typical current−voltage (*I*−*V*) characteristics of the SQ NW/*c*-Si heterojunction measured in darkness, revealing an excellent rectification behavior of the heterojunction with a rectification ratio (RR) up to 10^4 within ±3 V, and a low turn-on voltage of +1.2 V. It is noteworthy that the obtained RR value of $\sim 10^4$ has largely surpassed most reports on organic/inorganic *p*−*n* heterojunctions, such as CdS−polypyrrole (PPY) (RR = 13),[25] ZnO−poly(3-hexylthiophene) (P3HT) (RR = 5),[30] and CdS−polyaniline hybrid nanowire (RR = 35).[24] This is attributed to the high crystal quality of SQ NW, as well as the use of *c*-Si; less defects exist at the junction interface, so the leakage current is effectively suppressed in the reverse bias direction, leading to the improvement of RR. For an ideal diode, the rectification curve can be expressed using the following equation:[5]

$$I = I_0\left[\exp\left(\frac{qV}{nkT}\right) - 1\right] \approx I_0 \exp\left(\frac{qV}{nkT}\right) \quad (1)$$

where I_0 is the reverse saturation current, *n* the ideality factor, *q* the electronic charge, *k* the Bolzmann's constant, and *T* the absolute temperature. Based on the above equation, the ideality factor *n* can be deduced to be 1.03 in the low-bias zone (0−0.06 V) (see the inset in Figure 1e), which is in good agreement with the theoretical value (*n* = 1). In the higher-bias zone (0.07−0.2 V), however, the ideality factor increases to 3.4. This value is somewhat larger than the theoretical value at this regime (*n* = 2.0), implying the existence of impurities and defects at the organic NW/Si interface, which possibly formed during the solution growth process.[31]

Figure 1f depicts the absorption spectrum of the SQ NWs grown on Si substrate, along with the absorption spectra of the bare *n*-type Si substrate and the SQ NWs grown on a quartz substrate for comparison. Since the absorption of single SQ NW is too weak to detect, we increased the density of SQ NWs on the substrate with ∼50% NW coverage by adding the amount of SQ solution applied on the substrate to obtain a stronger signal (see Figure S3 in the Supporting Information). It is seen that the bare Si substrate has strong light absorption in the spectrum range of 600−1000 nm, while the SQ NWs (on quartz substrate) reveal relatively stronger absorption in the short wavelength direction in the range from UV to Vis. After growth of a layer of SQ NWs on the Si substrate, the combined system exhibits a broad spectral absorption ranging from UV to NIR with a high absorption coefficient. The unique optical properties of the formed *p*−*n* heterojunction make it a promising candidate for the applications in broadband photodetectors and solar cells.

Photodetection in the UV regime has drawn extensive attention, because of its wide applications in industry, instruments, and our daily life. UV light is typically divided into three spectral regimes: UV-C (for wavelengths between 280 nm and 200 nm), UV-B (for wavelengths between 320 nm and 280 nm), and UV-A (for wavelengths between 400 nm and 320 nm). Applications of Si in UV regime are normally hampered by the low light absorption (high reflectivity). Moreover, the small light transmission depth (<200 nm) for Si in the UV regime will induce strong surface recombination, leading to the degradation of device performance.[32] Figure 2a depicts the typical *I*−*V* curves of SQ NW/*c*-Si *p*−*n* heterojunction measured in darkness and under 0.66 mW/cm^2 light illumination with different UV excitation wavelengths of 254 nm (UV-C) and 302 nm (UV-B), respectively. Notably, the device exhibits pronounced response to the UV lights in the reverse-bias region. The photosensitivity (defined as $(I_{light} - I_{dark})/I_{dark}$) is as high as 430% for the device under the 254 and 302 nm light illumination at a bias voltage of −3 V. However, the photocurrent is nearly negligible in the forward bias region, up to +3 V. In order to assess the stability and reproducibility of the device, the UV lights were turned on/off manually (Figure 2b). It is seen that the device can follow the light change well, with a reasonable response time of ∼16 s for the rise/decay edges. The bias direction-dependent photoresponse is associated with the characteristics of the *p*−*n* junction; the built-in field (V_{bi}) in the reverse-bias region is much higher than that in the forward-bias region, and the space charge region is also wider (see Figures 2c and 2d). As a result, the photogenerated electron−hole pairs can be rapidly separated and collected by the electrodes in the reverse-bias region,

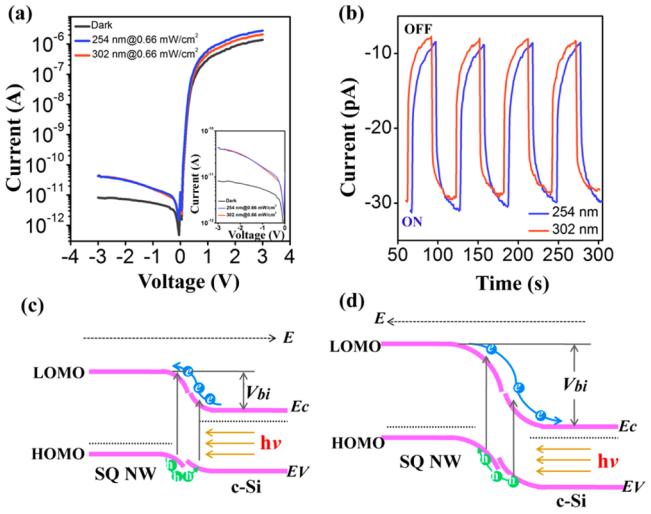

Figure 2. (a) *I*−*V* curves of SQ NW/*c*-Si heterojunction measured in darkness and under light irradiation of 254 and 302 nm lights, respectively; the inset shows the *I*−*V* curves of the reverse-bias region. (b) Time responses of the device to the pulsed incident light; the bias voltage was fixed at −3 V. Energy band diagrams of SQ NW/*c*-Si heterojunction in the (c) forward-bias region and (d) reverse-bias region. LOMO and HOMO represent the lowest unoccupied molecular orbital and the highest occupied molecular orbital, respectively. E_c and E_v are conduction band and valence band, respectively. *E* indicates the electric field in the heterojunction, and V_{bi} is the built-in electric field of the *p*−*n* heterojunction.

DOI: 10.1021/am5079144
ACS Appl. Mater. Interfaces 2015, 7, 2039−2045

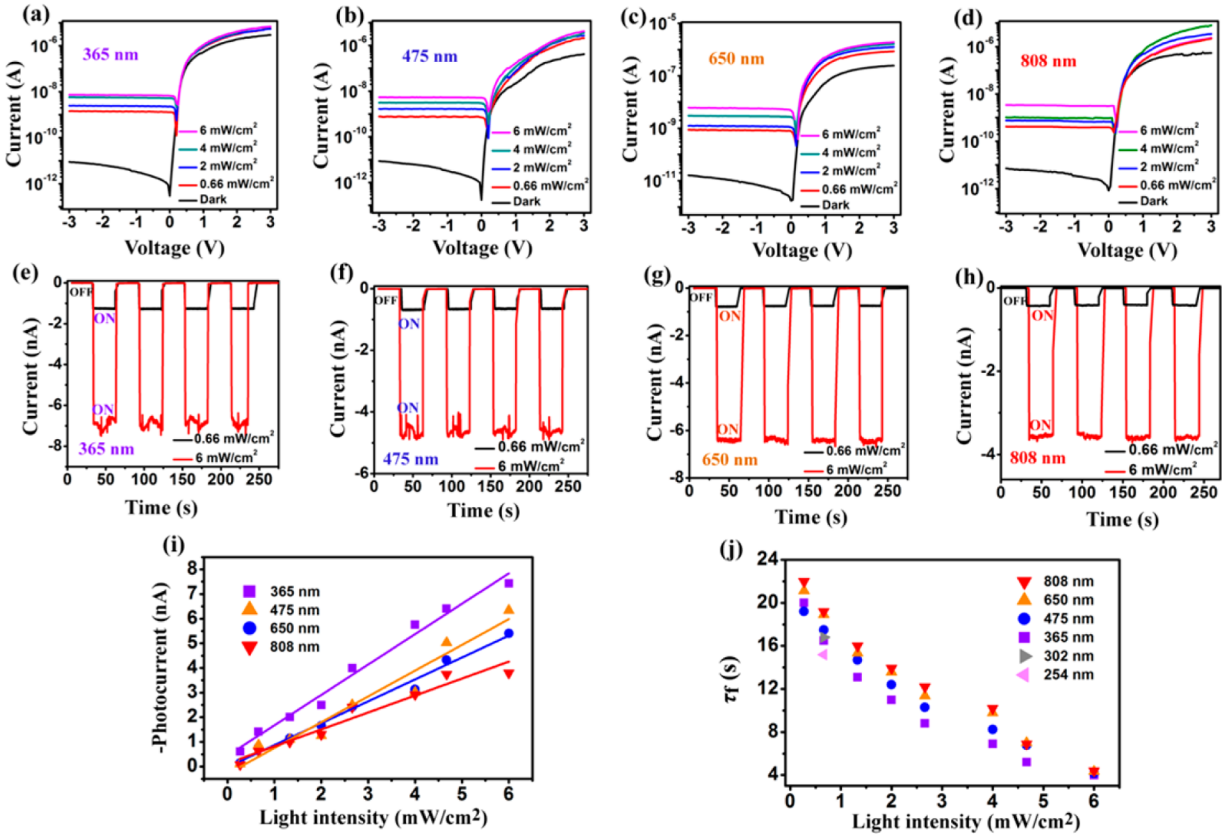

Figure 3. *I*–*V* curves of the device measured in darkness and under (a) 365 nm (UV light) irradiation, (b) 475 nm (Vis light) irradiation, (c) 650 nm (Vis light) irradiation, and (d) 808 nm (NIR light) irradiation with varied intensities. Time-resolved photoresponse of the device are shown in (e) 365 nm (UV light) irradiation, (f) 475 nm (Vis light) irradiation, (g) 650 nm (Vis light) irradiation, and (h) 808 nm (NIR light) irradiation with intensities of 0.66 and 6 mW/cm^2. Plots of the (i) photocurrent and (j) fall time (t_f), as a function of the light intensity under different excitation wavelengths (365, 475, 650, and 808 nm in panel (i), 254, 302, 365, 475, 650, and 808 nm in panel (j)). The bias voltage was fixed at −3 V.

leading to higher response speed and sensitivity. Also, the dark current is effectively suppressed in the reverse-bias direction, because of the existence of the junction barrier, which also contributes to the high photosensitivity. To further understand the significance of the *p*–*n* junction, we make a comparison between the *p*–*n* junction-type and ohmic-type photodetectors. The ohmic-type photodetectors were fabricated by drop-casting the SQ solution on the SiO_2/Si substrate with predefined Au electrode pairs (see Figure S4 in the Supporting Information). Under the same UV light illumination, however, the ohmic-type device exhibits much weaker photoresponse, with a small photosensitivity of ∼25%, in sharp contrast to that of the *p*–*n* junction-type device. In addition, the response speed of the ohmic-type device is obviously slower than that of the *p*–*n* junction-type device (see Figure S4b in the Supporting Information); the device can hardly reach the stable state, even after switching on/off the light for several tens of seconds, and the photocurrent tends to decrease as the operating time increases. The above results unambiguously prove the important role of the junction in enhancing the device performance. Based on the absorption spectra, we can also get the conclusion that the UV light response of the heterojunction should mainly come from the absorption of SQ NW in this regime.

To further evaluate the performance of the heterojunction-based photodetector from the UV-A regime, to the Vis regime, to the NIR regime, lights with four typical wavelengths of 365, 475, 650, and 808 nm were adopted as excitation sources, as shown in Figure 3. The *I*–*V* curves were measured under different excitation wavelengths (Figures 3a–d); meanwhile, the light intensities were tuned to investigate the intensity-dependent effect. It is found that the device exhibits a pronounced photoresponse on the selected wavelengths with excellent light-controlled characteristics at the reverse-bias direction. It is seen that the photocurrent rises up with the increase of the light intensity, revealing an approximately linear relationship (Figure 3i). The photosensitivities are deduced to be as high as 97 900%, 76 900%, 85 900%, and 68 000% for the 365, 475, 650, and 808 nm light, respectively, under the light intensity of 6 mW/cm^2. It is noteworthy that, because of the high photosensitivity, the *p*–*n* heterojunction device is capable of detecting light with intensity as low as 0.27 mW/cm^2, at which the photosensitivity remains as high as 7700%. We did not try a lower light intensity, because of the limitation of the light source. This characteristic is important for low-light detection and, therefore, demonstrates the great potential of developing low-light photodetectors based on the organic/inorganic heterojunctions. Figures 3e–h depict the time-resolved photoresponse of the device to the different excitation wavelengths at a fixed bias voltage of −3 V. It shows that the time response of the device illuminated with pulsed light is fast, highly stable, and reproducible. The *p*–*n* heterojunction device under the different excitation wavelengths of 365, 475, 650, and 808 nm exhibits an almost-identical rise time (t_r) of ∼0.6 s at the rise edges, while a relatively slower fall time (t_f) is observed at the decay edges. Therefore, it is believed that traps and other

DOI: 10.1021/am5079144
ACS Appl. Mater. Interfaces 2015, 7, 2039–2045

defect states are also involved in this process. Considering the high crystal quality of *c*-Si and the ultrafast photoresponse of commercial Si-based photodetectors (sub-nanosecond), the traps and defects are unlikely to come from the *c*-Si but may mainly exist in the SQ NW or at the junction interface. Under light illumination, the photogenerated carriers might first fill the traps and then reached the maximum level after all the traps were saturated, which induced a delay in reaching the steady photocurrent.[9] After switching off the light, however, the trapped carriers would gradually release from the traps. The detrapping process is slower than the filling process, thus leading to a relatively longer fall time. Figure 3j plots the relationship of t_f versus light intensity under different wavelengths. It is evident that the t_f decreases with increasing irradiation intensity. For the 365, 475, 650, and 808 nm lights, t_f decreases from ~20 s at 0.27 mW/cm^2 to ~4 s at 6 mW/cm^2. The reduction of the response time with increasing light intensity is in good agreement with previous investigations on inorganic nanostructures and can be interpreted according to Rose's model.[33] In Rose's model, it is assumed that traps are distributed with varying concentrations in the band gap. During light illumination, the semiconductor is not in a thermal equilibrium state, and excess electrons and holes are generated. Consequently, two quasi-Fermi levels are induced: one for electrons and another for holes. As the light intensity increases, the quasi-Fermi levels for electrons and holes shift toward the conduction and valence bands, respectively, and an increasing number of traps are converted to recombination centers. Thus, the t_f value is reduced significantly. In control experiments, the photoresponse of the ohmic-type device was also measured in UV-A light, visible light, and NIR light, as shown in Figure S5 in the Supporting Information. Similar to the investigation on UV-C and UV-B lights, the photoresponses of the ohmic-type device in these wavelength regimes are very weak, with poor stability and reproducibility.

From all the above results, it is clear that the SQ NW/*c*-Si *p*−*n* heterojunctions can serve as high-performance broadband photodetectors with detection range spanning from UV-C light, to UV-B light, to UV-A light, to Vis light, to NIR light. In order to quantitatively analyze the device performance, two of the important figures-of-merit parameters of a photodetector, i.e., photoresponsivity (R_λ) and photodetectivity (D^*), are further determined, according to the following equations:

$$R_\lambda = \frac{I_{light}}{PS} \tag{2}$$

$$D^* = \frac{R_\lambda}{(2qJ_d)^{0.5}} \tag{3}$$

where I_{light} is the photocurrent, P the incident light intensity, S the NW's effective illuminated area, and J_d the dark current density. S is equal to the contact area between SQ NW and Si substrate and is estimated to be 22.5 × 10^{-8} cm^2 through the expression

$$S = L \times D$$

where L is the length of the contacted part of the NW with the Si substrate (L= 45 μm), and D is the diameter of the NW (D = 500 nm). Figure 4a illustrates the wavelength-dependent R_λ and D^* of the heterojunction. Significantly, R_λ and D^* values of greater than 1.0 A/W and 6 × 10^9 Jones, respectively, in the wavelength range from 254 nm to 980 nm can be deduced, revealing the excellent device performance of the photo-

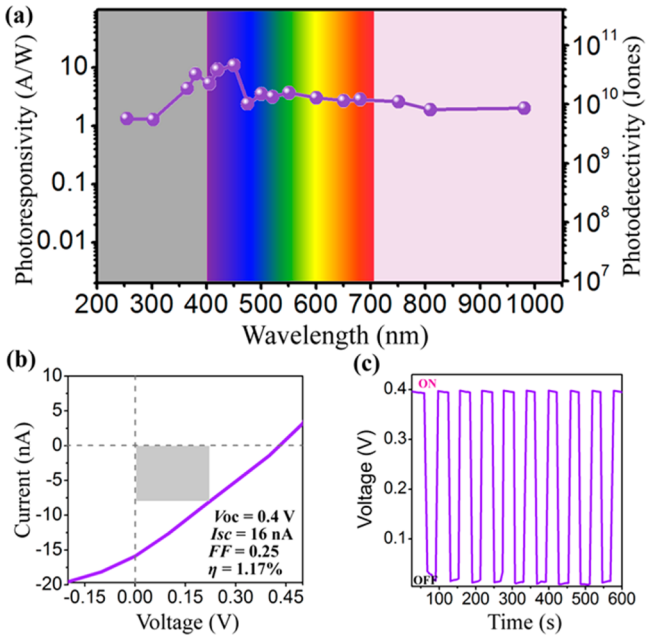

Figure 4. (a) Wavelength-dependent photoresponsivity and photodetectivity of the SQ NW/*c*-Si *p*−*n* heterojunction calculated at a fixed bias voltage of −3 V, revealing the broadband photoresponse of the heterojunction. (b) Photovoltaic characteristics of the SQ NW/*c*-Si heterojunction measured under AM 1.5G illumination (100 mW/cm^2). (c) Output voltage of the heterojunction, as a function of time, while the incident light was modulated.

detector. In addition, the light response of the device within the entire wavelength range is rather even with the device parameters on the same order. (The exceptional response band at ~450 nm is in accordance with the absorption peak of SQ NWs.) The flat photoresponse spectrum is vital to the broadband photodetector applications. It should be noted that the device performance of the SQ NW/*c*-Si *p*−*n* heterojunction is comparable or even superior to the reported broadband photodetectors fabricated from other inorganic or organic bulk heterojunctions (see Table 1).[34−37] The R_λ value (1.3−9.8 A/W) has surpassed the most reported values, highlighting the ultrahigh sensitivity of the SQ NW/*c*-Si *p*−*n* heterojunction. We note that the D^* value ((0.06−0.45) × 10^{11} Jones) is still lower than the best reported values ((12−100) × 10^{11} Jones for PDDTT/PC$_{60}$BM). Nevertheless, considering the fact that D^* is determined by the dark current to a large extent, it is expected that the photodetectivity can be readily improved in the future by further optimizing the device structure, as well as improving the junction quality. On the other hand, the broadband response of the SQ NW/*c*-Si heterojunction also makes it a promise candidate for solar cell applications. In this work, we have conducted a preliminary investigation on the photovoltaic characteristics of the device under AM 1.5G illumination at 100 mW/cm^2, as shown in Figure 4b. The device possesses an open-circuit voltage (V_{oc}) of ~0.4 V, a short-circuit current (I_{sc}) of ~1.6 × 10^{-8} A, and a fill factor (FF) of 0.25, yielding a power conversion efficiency (η) of ~1.17%. Notably, this η value is comparable to that of some reported organic/inorganic hybrid devices.[18,21,30,38,39] Figure 4c also shows the time response of the device measured at zero external bias voltage. The response of the device to pulsed light is fast with excellent stability and reproducibly, and the response time can be deduced below 4 s. Therefore, the device

DOI: 10.1021/am5079144
ACS Appl. Mater. Interfaces 2015, 7, 2039−2045

Table 1. Comparison of the Key Parameters of the SQ NW/*c*-Si Broadband Photodetector with Literature Data

photodetector	light [nm]	R_λ [A/W]	D^* @ V_{bia} [$\times 10^{11}$ Jones]	ref
SQ NW/*c*-Si	254−980	1.3−9.8	0.06−0.45 @ −3 V	this work
PDDTT/$PC_{60}BM$	300−1450	∼0.22	12−100 @ −100 mV	34
In_2Te_3 NW	350−1090	0.2−1.2		35
m-MTDATA/CuPc/$PTCDIC_8$	200−900	∼0.27	10 @ −3 V	36
SWCNTs/$PC_{71}BM$	400−1010	0.02−0.26	0.2−2 @ 0 V	37

has great potential to serve as self-powered photodetector operating at zero bias voltage.

The above results demonstrate the fascinating properties and tremendous application potential of the organic/inorganic heterojunctions fabricated from small-molecule organic NWs. Various potential improvements of the heterojunction design can be envisioned including the implementation of an ultrathin passivation layer on Si and the further reduction of defect states on organic NWs or at the organic/inorganic interface. It is known that the NW quality could be improved by optimizing the growth conditions or by post-growth annealing,[40] which is particularly important for the solution-grown organic nanostructures.[41] Also, in this work, a relatively large electrode pad with size of 200 μm × 200 μm was used, the large RC constant of the circuit will probably limit the device speed. Therefore, a smaller device size could be used to further improve the response speed of the device. This method with characteristics of one-step crystal growth and device fabrication, versatile room-temperature and solution process, could be readily extended to other small-molecule organic nanostructures. It will open up the opportunities for the construction of a variety of organic nanostructure/inorganic heterojunctions with unprecedented performance.

CONCLUSIONS

In summary, we fabricated single-crystal SQ NW/*c*-Si *p*−*n* heterojunctions via a simple drop-casting method. Their prospective applications in broadband photodetectors and solar cells were systematically studied. The photodetectors show ultrahigh sensitivity and broadband spectral response from the ultraviolet light regime, to the visible light regime, to the near-infrared light regime, because of the complementary spectrum absorption of SQ NWs with Si. The junction is vital to the improvement of device performance; the high built-in field, along with the effective suppression of dark current, gives rise to the ultrahigh sensitivity and fast response of the device in the reverse-bias region. Also, the pronounced photovoltaic behavior of the heterojunctions makes them promising candidates for self-powered photodetectors operating at zero external bias voltage. This new type of single-crystal organic NW/*c*-Si *p*−*n* heterojunction may have important applications in high-performance, low-cost broadband photodetectors and solar cells.

ASSOCIATED CONTENT

Supporting Information

Schematic illustration of the process used to fabricate SQ NW/Si heterojunctions, and the *I*−*V* characteristics of the SQ NW-based ohmic-type devices measured in darkness and under light illumination with different wavelengths (254, 302, 365, 475, 650, and 808 nm). This material is available free of charge via the Internet at http://pubs.acs.org.

AUTHOR INFORMATION

Corresponding Authors

*Tel.: +86-512-65881265. E-mail: jsjie@suda.edu.cn (J. S. Jie).
*Tel.: +86-512-65880955. E-mail: xjzhang@suda.edu.cn (X. J. Zhang).
*Tel.: +86-10-82543510. E-mail: xhzhang@mail.ipc.ac.cn (X. H. Zhang).

Author Contributions

The manuscript was written through contributions of all authors. All authors have given approval to the final version of the manuscript.

Notes

The authors declare no competing financial interest.

ACKNOWLEDGMENTS

This work was supported by the National Basic Research Program of China (Nos. 2013CB933500 and 2012CB932400), the Major Research Plan of the National Natural Science Foundation of China (Nos. 91233110 and 91333208), the National Natural Science Foundation of China (Nos. 51172151 and 51173124), the Natural Science Foundation of Jiangsu Province (No. BK20131162), and a Project Funded by the Priority Academic Program Development of Jiangsu Higher Education Institutions.

REFERENCES

(1) Yan, C. Y.; Wang, J. X.; Wang, X.; Kang, W. B.; Cui, M. Q.; Foo, C. Y.; Lee, P. S. An Intrinsically Stretchable Nanowire Photodetector with a Fully Embedded Structure. *Adv. Mater.* **2014**, *26*, 943−950.

(2) Lee, K. H.; Leem, D. S.; Castrucci, J. S.; Park, K. B.; Bulliard, X.; Kim, K. S.; Jin, Y. W.; Lee, S.; Bender, T. P.; Park, S. Y. Green-Sensitive Organic Photodetectors with High Sensitivity and Spectral Selectivity Using Subphthalocyanine Derivatives. *ACS Appl. Mater. Interfaces* **2013**, *5*, 13089−13095.

(3) Ihama, M.; Mitsui, T.; Nomura, K.; Maehara, Y.; Inomata, H.; Gotou, T.; Takeuchi, Y. CMOS Image Sensor with a Thin Overlaid Panchromatic Organic Photoconductive Layer for Sensors with Reduced Pixel Size. In *IDW '09, Proceedings of the 16th International Display Workshops*, Miyazaki, Japan, Dec. 9−11, 2009; Paper INP 1-4.

(4) Zhang, X. J.; Jie, J. S.; Zhang, W.; Zhang, C.; Luo, L.; He, Z.; Zhang, X. H.; Zhang, W. J.; Lee, C. S.; Lee, S. T. Photoconductivity of a Single Small-Molecule Organic Nanowire. *Adv. Mater.* **2008**, *20*, 2427−2432.

(5) Zhang, Y. P.; Deng, W.; Zhang, X. J.; Zhang, X. W.; Zhang, X. H.; Xing, Y. L.; Jie, J. S. In Situ Integration of Squaraine-Nanowire-Array-Based Schottky-Type Photodetectors with Enhanced Switching Performance. *ACS Appl. Mater. Interfaces* **2013**, *5*, 12288−12294.

(6) Wei, L.; Yao, J. N.; Fu, H. B. Solvent-Assisted Self-Assembly of Fullerene into Single-Crystal Ultrathin Microribbons as Highly Sensitive UV-Visible Photodetectors. *ACS Nano* **2013**, *7*, 7573−7582.

(7) Che, Y. K.; Yang, X. M.; Liu, G. L.; Yu, C.; Ji, H. W.; Zuo, J. M.; Zhao, J. C.; Zang, L. Ultrathin n-Type Organic Nanoribbons with High Photoconductivity and Application in Optoelectronic Vapor Sensing of Explosives. *J. Am. Chem. Soc.* **2010**, *132*, 5743−5750.

DOI: 10.1021/am5079144
ACS Appl. Mater. Interfaces 2015, 7, 2039−2045

(8) Liu, Y.; Wang, H. F.; Dong, H. L.; Jiang, L.; Hu, W. P.; Zhan, X. W. High Performance Photoswitches Based on Flexible and Amorphous D-A Polymer Nanowires. *Small* **2013**, *9*, 294−299.
(9) Deng, W.; Zhang, X. J.; Wang, J. C.; Shang, Q. X.; Gong, C.; Zhang, X. H.; Zhang, Q.; Jie, J. S. Very facile fabrication of aligned organic nanowires based high-performance top-gate transistors on flexible, transparent substrate. *Org. Electron.* **2014**, *15*, 1317−1323.
(10) Park, K. S.; Cho, B.; Baek, J.; Hwang, J. K.; Lee, H.; Sung, M. M. Single-Crystal Organic Nanowire Electronics by Direct Printing from Molecular Solutions. *Adv. Funct. Mater.* **2013**, *23*, 4776−4784.
(11) Kim, F. S.; Ren, G. Q.; Jenekhe, S. A. One-Dimensional Nanostructures of π-Conjugated Molecular Systems: Assembly, Properties, and Applications from Photovoltaics, Sensors, and Nanophotonics to Nanoelectronics. *Chem. Mater.* **2011**, *23*, 682−732.
(12) Wu, Y. M.; Zhang, X. J.; Pan, H. H.; Deng, W.; Zhang, X. H.; Zhang, X. W.; Jie, J. S. In-situ device integration of large-area patterned organic nanowire arrays for high-performance optical sensors. *Sci. Rep.* **2013**, *3*, 3248−3255.
(13) Zhao, Y. S.; Fu, H. B.; Peng, A. D.; Ma, Y.; Liao, Q.; Yao, J. N. Construction and Optoelectronic Properties of Organic One-Dimensional Nanostructures. *Acc. Chem. Res.* **2010**, *30*, 409−418.
(14) Zhao, Y. S.; Fu, H. B.; Peng, A. D.; Ma, Y.; Xiao, D. B.; Yao, J. N. Low-Dimensional Nanomaterials Based on Small Organic Molecules: Preparation and Optoelectronic Properties. *Adv. Mater.* **2008**, *20*, 2859−2876.
(15) Ma, D.; Aguiar, M.; Freire, J. A.; Hümmelgen, I. A. Organic Reversible Switching Devices for Memory Applications. *Adv. Mater.* **2000**, *12*, 1063−1066.
(16) Chu, C. W.; Ouyang, J. Y.; Tseng, J. H.; Yang, Y. Organic Donor-Acceptor System Exhibiting Electrical Bistability for Use in Memory Devices. *Adv. Mater.* **2005**, *17*, 1440−1443.
(17) Kim, S. J.; Lee, J. S. Flexible Organic Transistor Memory Devices. *Nano Lett.* **2010**, *10*, 2884−2890.
(18) Chang, J. A.; Rhee, J. H.; Im, S. H.; Lee, Y. H.; Kim, H. J.; Seok, S. I.; Nazeeruddin, M. K.; Gratzel, M. High-Performance Nanostructured Inorganic-Organic Heterojunction Solar Cells. *Nano Lett.* **2010**, *10*, 2609−2612.
(19) Plass, R.; Pelet, S.; Krueger, J.; Grätzel, M. Quantum Dot Sensitization of Organic−Inorganic Hybrid Solar Cells. *J. Phys. Chem. B* **2002**, *106*, 7578−7580.
(20) Wrightn, M.; Uddin, A. Solar Energy Materials and Solar Cells. *Sol. Energy Mater. Sol. Cells* **2012**, *107*, 87−111.
(21) Liu, Y. X.; Summers, M. A.; Edder, C.; Fréchet, J. M. J.; McGehee, M. D. Using Resonance Energy Transfer to Improve Exciton Harvesting in Organic−Inorganic Hybrid Photovoltaic Cells. *Adv. Mater.* **2005**, *17*, 2960−2964.
(22) Liu, J. P.; Wang, S. S.; Bian, Z. Q.; Shan, M.; Huang, C. H. Organic/inorganic hybrid solar cells with vertically oriented ZnO nanowires. *Appl. Phys. Lett.* **2009**, *94*, 173107.
(23) Guo, Y. B.; Tang, Q. X.; Liu, H. B.; Zhang, Y. J.; Li, Y. L.; Hu, W. P.; Wang, S.; Zhu, D. B. Light-Controlled Organic/Inorganic P−N Junction Nanowires. *J. Am. Chem. Soc.* **2008**, *130*, 9198−9199.
(24) Lin, H. W.; Liu, H. B.; Qian, X. M.; Lai, S. W.; Li, Y. J.; Chen, N.; Ouyang, C. B.; Che, C. M.; Li, Y. L. Constructing a Blue Light Photodetector on Inorganic/Organic *p*−*n* Heterojunction Nanowire Arrays. *Inorg. Chem.* **2011**, *50*, 7749−7753.
(25) Wang, L. D.; Zhao, D. X.; Su, Z. S.; Fang, F.; Li, B. H.; Zhang, Z. Z.; Shen, D. Z.; Wang, X. H. High spectrum selectivity organic/inorganic hybrid visible-blind ultraviolet photodetector based on ZnO nanorods. *Org. Electron.* **2010**, *11*, 1318−1322.
(26) Tang, Q. W.; Lin, L.; Zhao, X.; Huang, K.; Wu, J. H. p-n Heterojunction on Ordered ZnO Nanowires/Polyaniline Microrods Double Array. *Langmuir* **2012**, *28*, 3972−3978.
(27) Law, K. Y.; Bailey, F. C.; Bluett, L. J. Squaraine Chemistry. On the anomalous mass spectra of bis(4-dimethylaminophenyl)squaraine and its derivatives. *Can. J. Chem.* **1986**, *64*, 1607−1619.
(28) Zhang, C. Y.; Zhang, X. J.; Zhang, X. H.; Ou, X. M.; Zhang, W. F.; Jie, J. S.; Chang, J. C.; Lee, C. S.; Lee, S. T. Facile One-Step Fabrication of Ordered Organic Nanowire Films. *Adv. Mater.* **2009**, *21*, 4172−4175.
(29) Zhang, C. Y.; Zhang, X. J.; Zhang, X. H.; Fan, X.; Jie, J. S.; Chang, J. C.; Lee, C. S.; Zhang, W. J.; Lee, S. T. Facile One-Step Growth and Patterning of Aligned Squaraine Nanowires via Evaporation-Induced Self-Assembly. *Adv. Mater.* **2008**, *20*, 1716−1720.
(30) Briseno, A. L.; Holcombe, T. W.; Boukai, A. I.; Garnett, E. C.; Shelton, S. W.; Frechet, J. J. M.; Yang, P. D. Oligo- and Polythiophene/ZnO Hybrid Nanowire Solar Cells. *Nano Lett.* **2010**, *10*, 334−340.
(31) Wang, C. X.; Yang, G. W.; Liu, H. W.; Han, Y. H.; Luo, J. F.; Gao, C. X.; Zou, G. T. Experimental analysis and theoretical model for anomalously high ideality factors in ZnO/diamond *p*−*n* junction diode. *Appl. Phys. Lett.* **2004**, *84*, 2427.
(32) Sang, L. W.; Liao, M. Y.; Sumiya, M. A Comprehensive Review of Semiconductor Ultraviolet Photodetectors: From Thin Film to One-Dimensional Nanostructures. *Sensors* **2013**, *13*, 10482−10518.
(33) Jiang, Y.; Zhang, W. J.; Jie, J. S.; Meng, X. M.; Fan, X.; Lee, S. T. Photoresponse Properties of CdSe Single-Nanoribbon Photodetectors. *Adv. Funct. Mater.* **2007**, *17*, 1795−1800.
(34) Gong, X.; Tong, M. H.; Xia, Y. J.; Cai, W. Z.; Moon, J. S.; Cao, Y.; Yu, G.; Shieh, C. L.; Nilsson, B.; Heeger, A. J. High-Performance Organic Nanoscale Photoswitches Based on Nanogap Electrodes Coated with a Blend of Poly(3-hexylthiophene) and [6,6]-Phenyl-C_{61}-butyric Acid Methyl Ester (P_3HT:PCBM). *Science* **2009**, *325*, 1665−1648.
(35) Wang, Z. X.; Safdar, M.; Jiang, C.; He, J. High-Performance UV-Visible-NIR Broad Spectral Photodetectors Based on One-Dimensional In_2Te_3 Nanostructures. *Nano Lett.* **2012**, *12*, 4715−4721.
(36) Wu, S. H.; Li, W. L.; Chu, B.; Su, Z. S.; Zhang, F.; Lee, C. S. High performance small molecule photodetector with broad spectral response range from 200 to 900 nm. *Appl. Phys. Lett.* **2011**, *99*, 023305.
(37) Xie, Y.; Gong, M. G.; Shastry, T. A.; Lohrman, J.; Hersam, M. C.; Ren, S. Q. Broad-Spectral-Response Nanocarbon Bulk-Heterojunction Excitonic Photodetectors. *Adv. Mater.* **2013**, *25*, 3433−3437.
(38) Hau, S. K.; Cheng, Y. J.; Yip, H. L.; Zhang, Y.; Ma, H.; Jen, A. K. Y. Effect of Chemical Modification of Fullerene-Based Self-Assembled Monolayers on the Performance of Inverted Polymer Solar Cells. *ACS Appl. Mater. Interfaces* **2010**, *2*, 1892−1902.
(39) Kim, J. S.; Lee, J. H.; Park, J. H.; Shim, C.; Sim, M.; Cho, K. High-Efficiency Organic Solar Cells Based on Preformed Poly(3-hexylthiophene) Nanowires. *Adv. Funct. Mater.* **2011**, *21*, 480−486.
(40) Hu, Z.; Muls, B.; Gence, L.; Serban, D. A.; Hofkens, J.; Melinte, S.; Jonas, A. M. High-Throughput Fabrication of Organic Nanowire Devices with Preferential Internal Alignment and Improved Performance. *Nano Lett.* **2007**, *7*, 3639−3644.
(41) Li, H.; Tee, B. C. K.; Cha, J. J.; Cui, Y.; Chung, J. W.; Lee, S. Y.; Bao, Z. N. High-Mobility Field-Effect Transistors from Large-Area SolutionGrown Aligned C_{60} Single Crystals. *J. Am. Chem. Soc.* **2012**, *134*, 2760−2765.

DOI: 10.1021/am5079144
ACS Appl. Mater. Interfaces 2015, 7, 2039−2045